Journal of Applied Mathematics and Physics, 2025, 13(4), 1514-1522
https://www.scirp.org/journal/jamp
ISSN Online: 2327-4379
ISSN Print: 2327-4352

Numerical Study on the Two-Dimensional Self-Propulsion of a Hydrofoil

Yusheng Liu, Tao Zhou, Xingjian Lin*

School of Mechanical Engineering, Nanjing Institute of Technology, Nanjing, China
Email: *xjlinf@njit.edu.cn

How to cite this paper: Liu, Y.S., Zhou, T. and Lin, X.J. (2025) Numerical Study on the Two-Dimensional Self-Propulsion of a Hydrofoil. *Journal of Applied Mathematics and Physics*, **13**, 1514-1522.
https://doi.org/10.4236/jamp.2025.134081

Received: March 28, 2025
Accepted: April 22, 2025
Published: April 25, 2025

Abstract

The underlying mechanisms driving the efficient propulsion of fish remain incompletely understood. In this study, fish is simplified as hydrofoil with two degrees of freedom in two-dimensional flow, the effects of flapping frequency and wavelength on propulsion performance of a hydrofoil are numerically studied. It is found that the propulsion velocity increases monotonically with the rise of frequency, while it varies non-linearly with wavelength variation. However, the efficiency demonstrates contrasting trends—increasing monotonically with frequency elevation while decreasing progressively with wavelength extension. Notably, optimal performance is achieved at a flapping frequency of $f = 2$ and wavelength $\lambda = 1.5$. The results here may shed some lights on the understanding of the efficient swimming of fish.

Keywords

Fish Swimming, Fluid Simulation

1. Introduction

The efficient swimming of fish in nature has attracted the attention of researchers for a large time. However, the fluid mechanics behind the efficient swing of fish is still lack of fully explored. Fluid simulation technology plays a pivotal role in robotic fish development, enabling researchers to gain profound insights into fluid-structure interactions and subsequently optimize design parameters and performance characteristics.

Numerous studies have investigated hydrodynamic effects on robotic fish performance. Smith *et al.* employed numerical simulations to analyze how different swimming modes affect propulsion efficiency, revealing that undulation frequency and amplitude significantly influence propulsion forces [1]. Jones *et al.* examined flow field structures' impact on stability, proposing streamlined shape

optimizations for drag reduction [2]. Wang *et al.* experimentally validated energy consumption characteristics across velocity ranges, establishing critical references for energy efficiency optimization [3].

Recent advancements include Yikun Feng and colleagues' numerical investigation of self-propelled fin hydrodynamics, demonstrating significant variations in swimming performance induced by differences in fin morphology [4]. May Hlaing Win Khin and colleagues conducted three-dimensional fluid-structure interaction simulations of flexible caudal fins with varying trailing-edge configurations, providing a detailed study of the thrust characteristics and flow fields around each fin [5]. Qingyang Zhao and colleagues conducted numerical simulations of biomimetic swimmers with crescent-shaped caudal fins, exploring their propulsion performance during acceleration and cruising motions [6].

While existing literature has examined various propulsion efficiency factors including swimming modes, flow structures, fin morphologies, and material compliance. However, the two-dimensional self-propulsion is neglected in the previous studies. In this paper, fish is simplified as a hydrofoil, which self-propel in both longitudinal and lateral directions. The effects of frequency and wavelength on the propulsion are numerically studied.

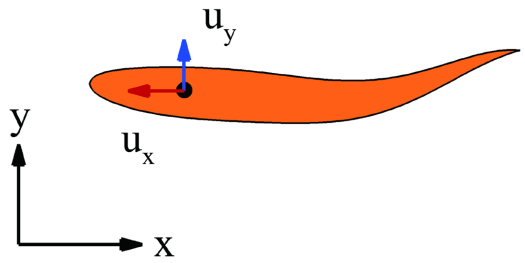

Figure 1. Sketch view of the simulation model.

2. Problem Description and Methodology

In this paper, fish is simplified as a two-dimensional undulating hydrofoil, as shown in **Figure 1**. The undulation motion along the fish body is prescribed as

$$y_0\left(\frac{x}{L},t\right)=A\left(\frac{x}{L}\right)\cos\frac{2\pi}{\lambda}\left(\frac{x}{L}-ct\right) \tag{1a}$$

$$A\left(\frac{x}{L}\right)=a_0-a_1\frac{x}{L}+a_2\left(\frac{x}{L}\right)^2,0\le\frac{x}{L}\le 1 \tag{1b}$$

where y_0 is the vertical displacement of the middle-line along the fish body, $A(x/L)$ represents the undulated amplitude along the fish body, L shows the length of the fish body, t is the time, λ and c denote the wavelength and the phase speed respectively, and $a_0 = 0.02$, $a_1 = 0.0825$, and $a_2 = 0.1625$.

The hydrofoil can self-propel in both the x and y directions. Its propulsion is governed by Newton's second law, which can be described as follows.

$$m\frac{\mathrm{d}^2X}{\mathrm{d}t^2}=F \tag{2}$$

where $X=(X,Y)$ is the position vector of the hydrofoil, and $F=(F_x,F_y)$ is the hydrodynamic force applied on the foil surface. m is the mass of the foil; t is the time. The cycle-averaged speeds of the foil in the x- and y-directions, respectively, can be calculated as

$$\begin{aligned}\overline{u}_x &= \frac{1}{T}\int_0^T u_x \mathrm{d}t = \frac{1}{T}\int_0^T (\mathrm{d}X/\mathrm{d}t)\mathrm{d}t \\ \overline{u}_y &= \frac{1}{T}\int_0^T u_y \mathrm{d}t = \frac{1}{T}\int_0^T (\mathrm{d}Y/\mathrm{d}t)\mathrm{d}t\end{aligned} \tag{3}$$

where T is the wave period of the foil. The cycle-averaged power consumption of the foil is defined as

$$\begin{aligned}\overline{P} &= \frac{1}{T}\int_0^T \left(F_y \frac{\mathrm{d}y}{\mathrm{d}t}\right)\mathrm{d}t \\ \overline{C_p} &= \overline{P}/\left(0.5\rho c u^3\right)\end{aligned} \tag{4}$$

The 2D flow can be described as N-S equation.

$$\frac{\partial u}{\partial t} + u * \nabla u = -\frac{1}{\rho}\nabla p + v\nabla^2 u \tag{5a}$$

$$\nabla * u = 0 \tag{5b}$$

where ρ represents fluid density, u is the velocity vector, p denotes pressure, v is the kinematic viscosity of the flow. A simplified circular function-based gas kinetic method [7] is used to solve the Navier-Stokes equation, and the implicit velocity correction-based immersed boundary [8] is used to resolve the interaction between the flapping foil and the surrounding flow. The method and the corresponding code have been developed to efficiently solve the governing equations of motion and fluid dynamics, enabling the simulation of the hydrofoil's undulating motion. And the corresponding method has been validated for flapping foil simulations over a wide range of kinematics [9]-[11].

3. Results and discussion

To gain a deeper understanding of the hydrodynamics of fish swing. The cycle-averaged speed, energy consumption, and the efficiency of the hydrofoil are calculated, respectively. Moreover, the wake characteristics of hydrofoil is analyzed. All simulations in this study were conducted over 25 cycles to ensure the convergence of the results. The values of f and λ range from 0.5 to 3.

In the simulations here, the hydrofoil has self-propulsion along x-direction, and the cycle-averaged speed in the lateral direction is zero. Thus, only the cycle-averaged speed in the x-direction is described here.

$$\overline{u_x} = \frac{1}{T}\int_0^T u_x \mathrm{d}t \tag{6}$$

In the equation, T represents the duration of one cycle, while u_x denotes the instantaneous speed value at each data point.

As shown in **Figure 2(a)**, for a fixed wavelength, the propulsion speed of hydrofoil increases monotonically with the increase in oscillation frequency. Clearly,

a higher oscillation frequency allows hydrofoil to achieve a faster propulsion speed.

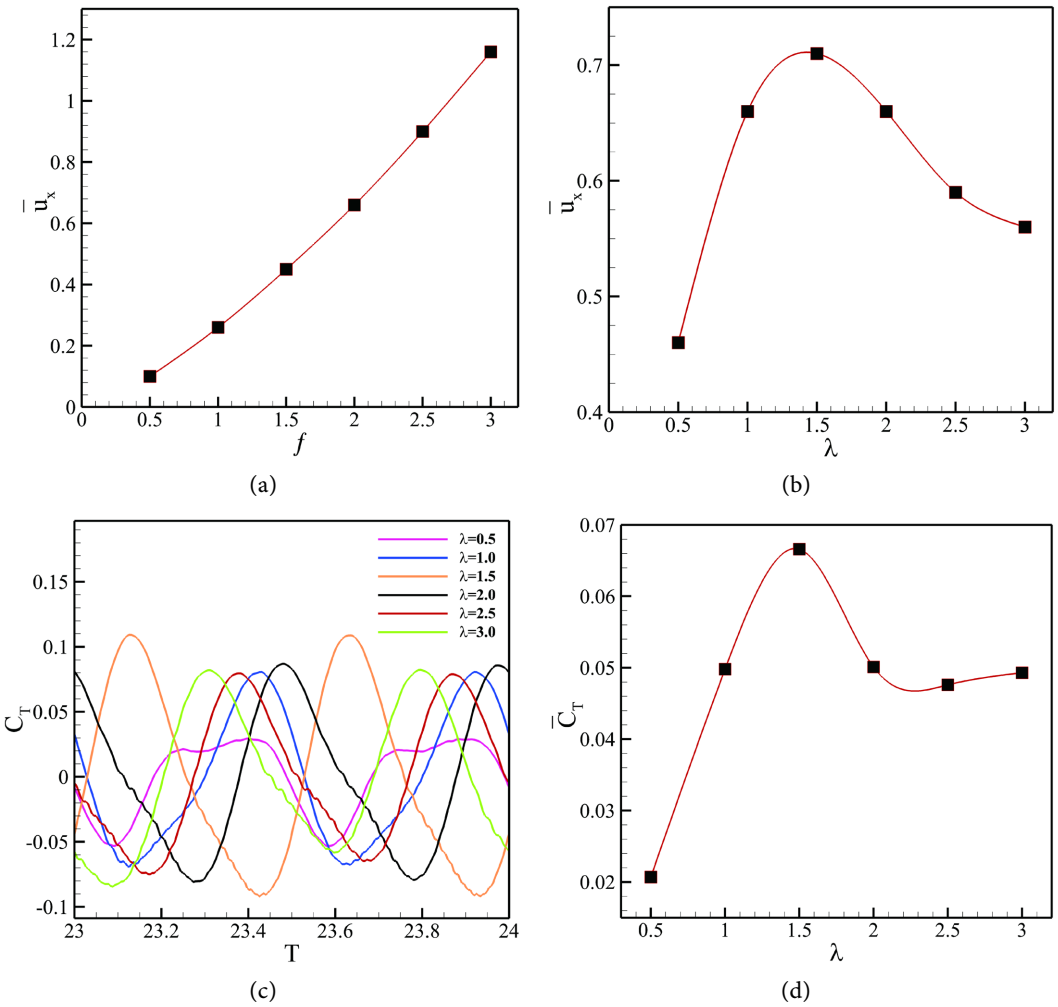

Figure 2. (a) The cycle-averaged speed as a function of frequency, $\lambda = 1$. (b) The cycle-averaged speed as a function of oscillation wavelength, $f = 2$. (c) The thrust curves of hydrofoil in different cases, $\lambda : (0.5 \sim 3.0)$. (d) The cycle-averaged values of positive thrust coefficient in different cases, $\lambda : (0.5 \sim 3.0)$.

On the other hand, as shown in **Figure 2(b)**, at a fixed oscillation frequency, the propulsion speed of hydrofoil initially increases and then decreases as the wavelength increases. The maximum propulsion speed is achieved at $\lambda = 1.5$, after which the propulsion speed decreases with further increases in wavelength. As can be seen from **Figure 2(c)** and **Figure 2(d)**, the thrust increases with increasing wavelength, reaches its maximum at 1.5, and then decreases. The greater the thrust, the faster the speed.

Indeed, the cycle-averaged speed of the undulating hydrofoil is an important parameter, as it allows for the assessment of the hydrofoil's dynamic performance. The fluctuation of speed is a key to understand the hydrodynamic characteristics and optimizing the design. A smaller velocity oscillation amplitude indicates bet-

ter fluid dynamic stability during swimming, suggesting that the interaction between the fluid and hydrofoil is minimal. Conversely, a larger velocity oscillation amplitude indicates poorer fluid dynamic stability, implying a greater interaction between the fluid and hydrofoil.

According to relevant statistical formulas, the equation for calculating the oscillation amplitude of velocity is as follows:

$$\Delta u = \frac{\left| u_{x\max} - u_{x\min} \right|}{2} \tag{7}$$

As shown in Figure 3(a), through periodic calculations and analysis, the velocity oscillation amplitude exhibits an overall increasing trend with the growth of the oscillation frequency f. Notably, at an oscillation frequency of $f = 2$, the rate of increase in velocity oscillation amplitude further accelerates. This indicates that when the wavelength λ is held constant, the velocity oscillation amplitude increases as the oscillation frequency f rises. As shown in Figure 3(b), when the oscillation frequency f is held constant, the velocity oscillation amplitude initially increases with the wavelength λ. It reaches a maximum value at $\lambda = 1.5$, followed by a brief decline before continuing to increase slowly. As shown in Figure 2(c), at a wavelength of 1.5, the thrust oscillation amplitude is the largest, leading to the maximum speed oscillation amplitude.

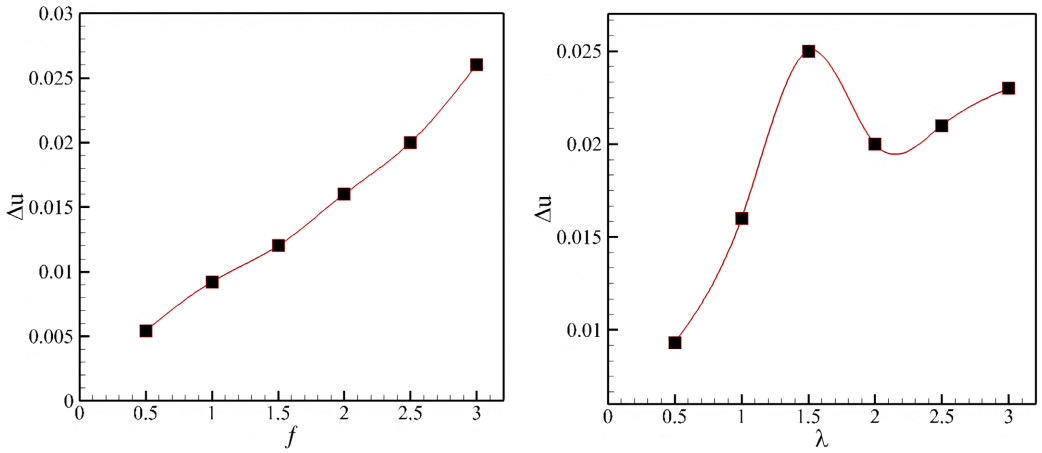

Figure 3. (a) The velocity oscillation amplitude versus frequency f. (b) The velocity oscillation amplitude versus wavelength λ.

The impact of frequency and wavelength on the energy consumption of the hydrofoil is shown in Figure 4. Firstly, as shown in Figure 4(a), as the oscillation frequency increases, the energy consumption coefficient also rises, exhibiting a monotonically increasing trend. At lower frequencies (from 0.5 to 1.5), the growth of the energy consumption coefficient is relatively slow, while at higher frequencies (from 1.5 to 3), the rate of increase accelerates. This suggests a potential for continued growth. Secondly, as shown in Figure 4(b), it can be observed that

when the oscillation frequency is fixed, the energy consumption coefficient increases with the increase of the wavelength. At smaller values of λ (from 0.5 to 1.5), the growth of the energy consumption coefficient is quite pronounced; however, the rate of increase slows down thereafter, approaching a limiting value. This indicates that as the wavelength increases, the energy consumption coefficient also rises, but the degree of change diminishes, converging towards a constant value.

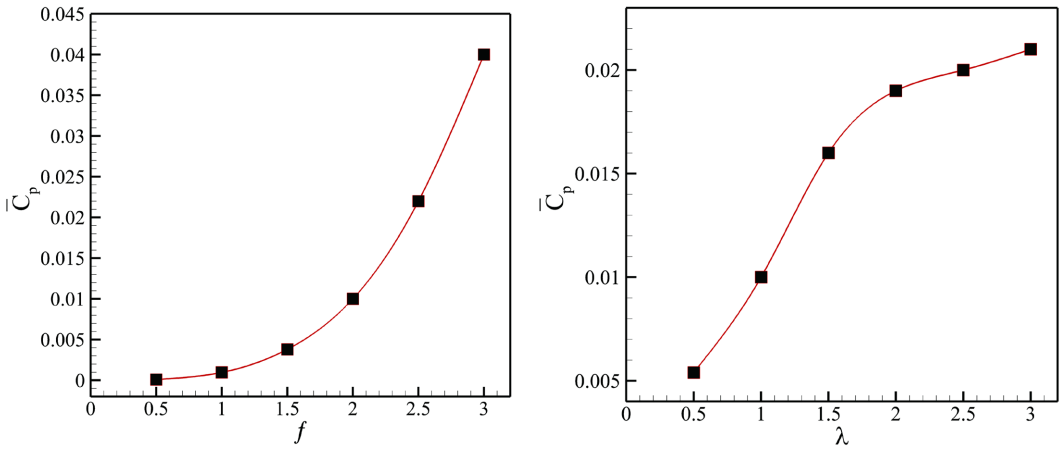

Figure 4. (a) The impact of frequency f on energy consumption. (b) The impact of wavelength λ on energy consumption.

The propulsion efficiency is the most intuitive parameter among all the indicators. The calculation formula is as follows:

$$\eta = \frac{1}{2}\left(1 + \frac{u_x}{f}\right) \tag{8}$$

In the equation, u_x represents the average speed of the robotic fish, and f denotes the speed of the backward undulating body wave.

As shown in **Figure 5**, for a fixed wavelength, the propulsion speed of the hydrofoil increases monotonically with the increase in oscillation frequency, although the rate of increase diminishes. On the other hand, for a fixed oscillation frequency, the propulsion efficiency decreases monotonically with increasing wavelength.

As shown in **Figures 6(a)-(c)**, for a fixed wavelength, the intensity of the tail vortices gradually increases with the rise in frequency, leading to a stronger reverse Kármán vortex street in the wake. However, there is no observed inclination of the tail's reverse Kármán vortex street.

On the other hand, as illustrated in **Figures 6(d)-(f)**, for a fixed oscillation frequency, the vortex structure at the tail of hydrofoil progressively strengthens with increasing oscillation wavelength. Notably, at $f = 2$ and $\lambda = 2.5$, a significant inclination of the tail's reverse Kármán vortex street occurs, as shown in **Figure 6(f)**. This indicates a tendency for lateral yaw motion, which is unfavorable for the cruising state of hydrofoil. Therefore, to avoid the inclination of the tail vorti-

ces, it is advisable to select a relatively smaller wavelength. For instance, when the fixed oscillation frequency is $f = 2.0$, the wavelength of hydrofoil should not exceed 2.5.

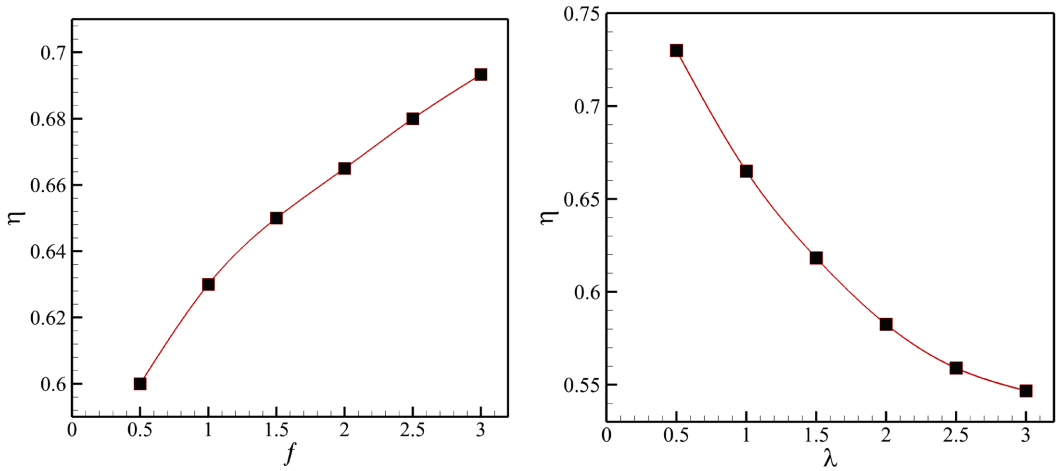

(a) (b)

Figure 5. (a) The propulsion efficiency varying with wave frequency. (b) The propulsion efficiency varying with oscillation wavelength.

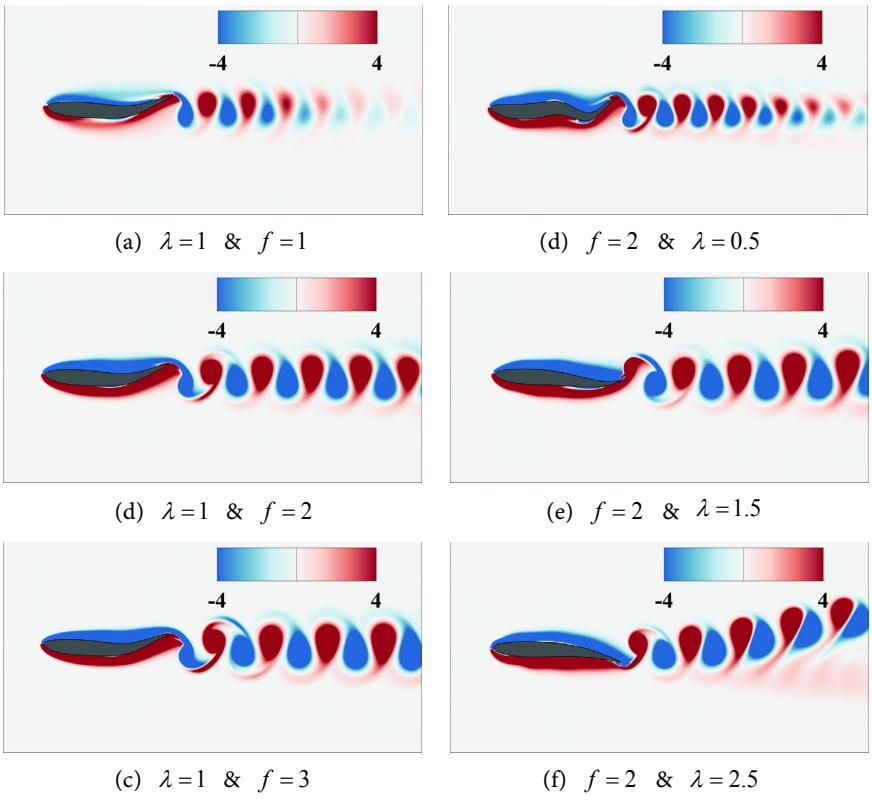

(a) $\lambda = 1$ & $f = 1$ (d) $f = 2$ & $\lambda = 0.5$

(d) $\lambda = 1$ & $f = 2$ (e) $f = 2$ & $\lambda = 1.5$

(c) $\lambda = 1$ & $f = 3$ (f) $f = 2$ & $\lambda = 2.5$

Figure 6. Instantaneous vorticity contours of the hydrofoil with different parameters.

As shown in **Figures 7(a)-(c)**, as the frequency increases, the pressure fluctua-

tions may increase and the vortex generation cycle is shortened, resulting in more complex flow separation phenomena. Wavelength tuning optimizes vortex energy distribution, with medium wavelength ($\lambda = 1.5$) being a key parameter for thrust performance and flow stability.

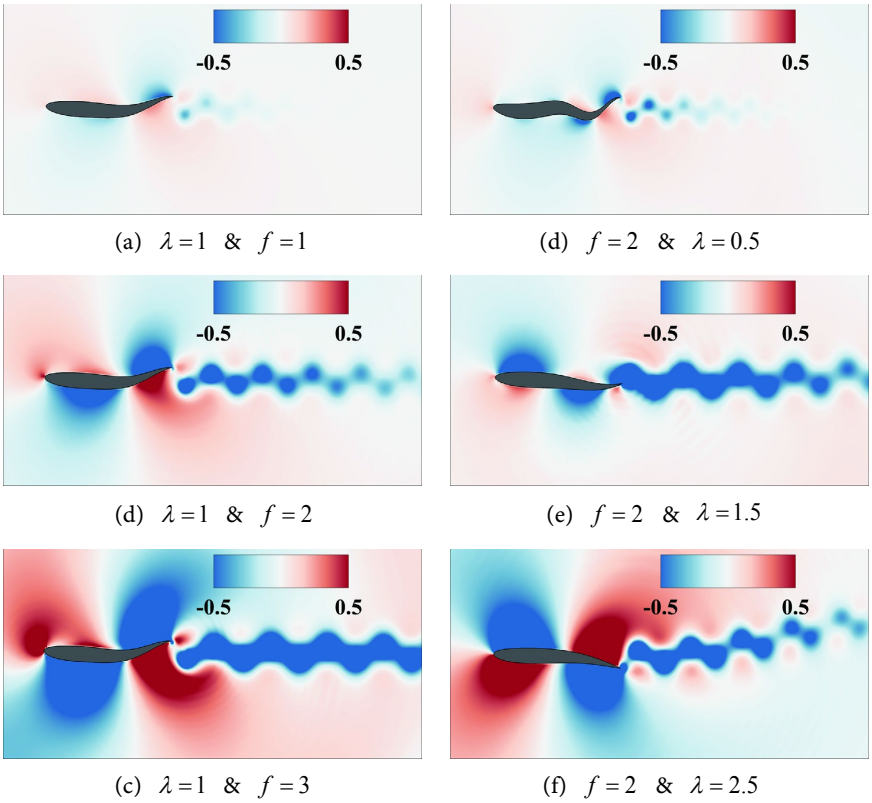

Figure 7. Instantaneous pressure contours of the hydrofoil with different parameters.

4. Conclusion

In this paper, fish are simplified as biomimetic fish with two degrees of freedom. The effects of flapping frequency and wavelength on their propulsion efficiency are studied through numerical simulations. It is found that when the flapping frequency $f = 2$ and the wavelength $\lambda = 1.5$, the fish can achieve a fast swimming speed while maintaining excellent efficiency. Additionally, at larger wavelengths, a phenomenon of tail vortex inclination occurs. These findings not only enhance our understanding of animal locomotion but also provide valuable insights for the design of biomimetic and autonomous swimming robots.

Acknowledgments

X.L. acknowledges the support of the Natural Science Foundation of Jiangsu Province (Grant No. BK20220686), and the Scientific Research Foundation of Nanjing Institute of Technology (Grant No. YKJ202221).

Conflicts of Interest

The authors declare no conflicts of interest regarding the publication of this paper.

References

[1] Smith, S.M., Venning, J.A., Pearce, B.W., Young, Y.L. and Brandner, P.A. (2020) The Influence of Fluid-Structure Interaction on Cloud Cavitation about a Stiff Hydrofoil. Part 1. *Journal of Fluid Mechanics*, **896**, A1. https://doi.org/10.1017/jfm.2020.321

[2] Jones, L. and White, R. (2021) Flow Field Analysis of Bio-Inspired Fish Robots: Stability and Performance. *International Journal of Robotics Research*, **40**, 567-580.

[3] Wang, Y., Zhang, H. and Li, X. (2022) Energy Consumption Characteristics of Bio-inspired Robotic Fish at Varying Speeds. *Robotics and Autonomous Systems*, **145**, 103-115.

[4] Feng, Y., Xu, J. and Su, Y. (2023) Effect of Trailing-Edge Shape on the Swimming Performance of a Fish-Like Swimmer under Self-propulsion. *Ocean Engineering*, **287**, Article 115849. https://doi.org/10.1016/j.oceaneng.2023.115849

[5] Khin, M.H.W. and Obi, S. (2024) Numerical Study on the Hydrodynamic Performance of a Flexible Caudal Fin with Different Trailing-Edge Shapes. *Biomimetics*, **9**, Article 445. https://doi.org/10.3390/biomimetics9070445

[6] Zhao, Q., Li, R., Liu, Y. and Guo, C. (2024) Numerical Simulation on the Propulsion Performance of a Bioinspired Swimmer with Crescent-Shaped Caudal Fin during Accelerating and Cruising Motion. *Ocean Engineering*, **306**, Article 118151. https://doi.org/10.1016/j.oceaneng.2024.118151

[7] Yang, L.M., Shu, C., Yang, W.M., Wang, Y. and Wu, J. (2017) An Immersed Boundary-Simplified Sphere Function-Based Gas Kinetic Scheme for Simulation of 3D Incompressible Flows. *Physics of Fluids*, **29**, Article 083605. https://doi.org/10.1063/1.4997085

[8] Wu, J. and Shu, C. (2009) Implicit Velocity Correction-Based Immersed Boundary-Lattice Boltzmann Method and Its Applications. *Journal of Computational Physics*, **228**, 1963-1979. https://doi.org/10.1016/j.jcp.2008.11.019

[9] Lin, X., Liu, Y. and Wu, J. (2024) Various and Orderly Formations in the Hydrodynamic Schooling of Multiple Flapping Swimmers. *Physics of Fluids*, **36**, Article 081902. https://doi.org/10.1063/5.0219371

[10] Lin, X., Wu, J. and Zhang, T. (2020) Self-Directed Propulsion of an Unconstrained Flapping Swimmer at Low Reynolds Number: Hydrodynamic Behaviour and Scaling Laws. *Journal of Fluid Mechanics*, **907**, R3. https://doi.org/10.1017/jfm.2020.955

[11] Lin, X., Zhou, T., Liu, Y. and Wu, J. (2025) A Sudden Alteration in the Self-Propulsion of Tandem Flapping Foils. *Physics of Fluids*, **37**, Article 021915. https://doi.org/10.1063/5.0256097